Magnetic-field tuning of domain-wall multiferroicity

R. M. Vakhitov [ORCID],[1] R. V. Solonetsky [ORCID],[1] V. R. Gurjanova,[2] A. R. Nizjamova,[1] D. A. Sechin,[3]
T. T. Gareev [ORCID],[3,4,*] and A. P. Pyatakov [ORCID][3]

[1]*Theoretical Physics Department, Physics and Technology Faculty, Bashkir State University, 450076 Ufa, Russia*
[2]*Management Department in the Internal Affairs, Ufa Law Institute, 450103 Ufa, Russia*
[3]*Oscillation Department, Physical Faculty, Lomonosov Moscow State University, 119991 Moscow, Russia*
[4]*Institute for Molecules and Materials, Radboud University, 6525AJ Nijmegen, the Netherlands*

Néel-type magnetic domain walls locally reduce the symmetry of the crystal and give rise to electric polarization. This type of localized multiferroicity is particularly promising due to the sensibility of the domain wall's internal structure to the magnetic field. In this paper, the magnetic-field-modified electric polarization of the domain wall is considered and compared to the room-temperature giant magnetoelectric effect observed on domain walls in iron garnet films.

I. INTRODUCTION

Magnetoelectric coupling in multiferroic materials with coexisting ferroelectric and magnetic ordering is now an issue of keen interest from a fundamental point of view [1,2] as well as from practical standpoints since it offers a low-energy-consuming way in spin electronics and magnetic storage [3–5].

Recently, local ferroelectricity of a micromagnetic origin, i.e., electric polarization related to a micromagnetic configuration rather than to a chemical composition or crystal structure, has been found [6,7]. The local symmetry violation due to spatial spin modulation results in the electric polarization of micromagnetic structures such as bubble domains [8], domain walls [9], Bloch lines [10], and magnetic vortices and skyrmions [10–12].

The mobility of these structures and their easy transformation in a magnetic field resulted in magnetic-field-controlled electric polarization, a particularly promising approach to the problem of scarcity of single-phase room-temperature magnetoelectric materials.

Understanding the correlation between a micromagnetic structure and its electric polarization is a prerequisite for the usage of this local type of multiferroicity. Earlier, a magnetic-field-induced switching of the electric-field polarity of the domain walls in iron garnet films was observed and analyzed in terms of domain structure topology [13]. However, there is still no theoretical model for the dramatic enhancement (an order of value) of domain-wall magnetoelectricity by an in-plane magnetic field [6,13]. To analyze the dependence of the magnetoelectric properties on a bias magnetic field the internal micromagnetic structure of the domain wall and its transformation in the field should be considered.

In this paper, a theoretical model for an electric polarization associated with a magnetic domain wall is proposed and is proven on the experimental data on giant magnetoelectric effect in iron garnet films. This model enables us to explain the observed effect of the magnetic-field-induced enhancement of domain-wall magnetoelectricity, as well as the magnetic-field-induced switching of the electric polarity of the domain wall and the saturation of its magnetoelectric polarization in a high magnetic field.

II. EXPERIMENT

A conceptual scheme of the experiment is presented in Fig. 1. We placed a point electrode in the vicinity of the stripe domain wall and applied an electric voltage between the electrode and film substrate that resulted in the displacement of the electrically polarized domain walls due to electrostatic forces. When the voltage was switched off the domain walls returned to their equilibrium positions.

The samples used in the experiments were iron garnet films $(BiLu)_3(FeGa)_5O_{12}$ epitaxially grown on (210) $Gd_3Ga_5O_{12}$ substrates (the details of the growth technique can be found elsewhere [14]). The parameters of the samples can be found in Table I. The domain structure of the samples was visualized by a magneto-optical technique in the Faraday mode. All measurements were carried out at room temperature.

The displacement caused by the electric probe served as a measure of the domain-wall magnetoelectricity. Since our samples are magnetically soft and domain walls are very mobile and sensitive to external influences, the standard scanning probe microscopy technique cannot be used to detect the position of the domain wall. Owing to the large-scale domain structure the displacement of the domain wall can be measured by nondisturbing magneto-optical means: by subtracting the magneto-optical images of the domain structure in the electric field and in the initial (zero electric field) state (Fig. 2).
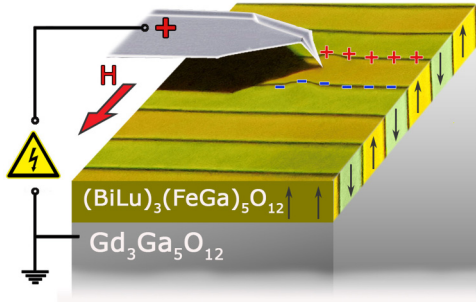
*Corresponding author: timur.gareev@ru.nl

FIG. 1. The scheme of the experiment. As the electric-field source an electrically biased visual contact silicon cantilever tip was used [VIT_P_C-A (NT-MDT)] touching the surface of the sample. The tip potential $U = 500$ V, and electric field at the tip $E \sim 1$ MV/cm.

In the absence of a magnetic field, all domain walls were attracted by a positively biased electrode (and repelled from a negatively charged one [9]), that evidenced for some "built-in" polarity of domain walls in a spontaneous domain structure due to the inversion symmetry breaking in the films. The inversion symmetry violation in epitaxially grown iron garnet film samples is a well-established fact confirmed by the linear electro-magneto-optical effect [15] and second harmonic optical generation [16].

For symmetrical arguments when the external magnetic field perpendicular to the domain wall is applied, the adjacent domain walls are no longer equivalent. For a given domain wall the attraction to the charged tip either enhances or reduces depending on the sign of the magnetic-field projection on [001] axis (directed to the right or left in Fig. 2). In the case of the reduction, the magnetoelectric effect vanishes at some critical value H_0 and transforms to an *electric-field-induced repulsion* that increases with an increasing absolute value of the field. Thus, in a magnetic field higher than the critical one, the adjacent domain walls have opposite electric polarities: One is attracted to the tip, another is repelled from it (Figs. 1 and 2).

To understand this intricate modification of the domain-wall magnetoelectricity, we suggest the model based on the concept of an inhomogeneous magnetoelectric interaction [17].

III. MODEL

The inhomogeneous magnetoelectric interaction is a variety of magnetoelectric coupling associated with magnetic inhomogeneities [17] that is expressed in terms of the

TABLE I. Parameters of the studied samples. D is the film thickness, M_s is the saturation magnetization, and λ is the period of the domain structure.

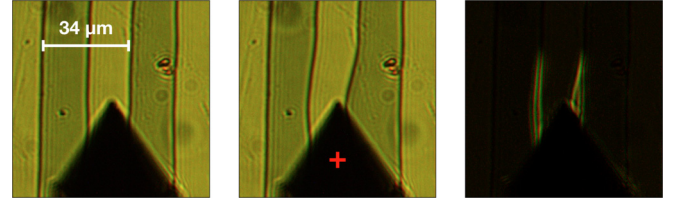| Sample	D (μm)	$4\pi M_s$ (G)	λ (μm)
1	10.0	54	34
2	7.4	77	44

FIG. 2. Electric-field-induced domain-wall displacement: The left figure corresponds to the initial domain structure; the central photograph shows the distortion of the domain structure in the electric field of the tip electrode; the right picture is the result of the image subtraction of the two photographs. A bias in-plane magnetic field $H = 80$ Oe directed along [001] axis, from left to right is applied. Sample 1 from Table I is used as an illustration.

Lifshitz invariant [18]

$$\varepsilon_{ME} = M_s^2 \mathbf{P}(\gamma_1 \mathbf{m} \operatorname{div} \mathbf{m} + \gamma_2 \mathbf{m} \times \operatorname{rot} \mathbf{m}), \quad (1)$$

where M_s is spontaneous magnetization, $\mathbf{P}||Oz$ parallel to the film normal is spontaneous electric polarization associated with inversion symmetry breaking in a magnetic film, γ_1 and γ_2 are magnetoelectric constants [18,19], and $\boldsymbol{m}$ is the unit magnetization vector.

The geometry of the problem is shown in Fig. 3. The easy axis of a uniaxial ferromagnet is directed along the normal to the film and parallel to the Oz axis; the Oy axis coincides with the direction of magnetization modulation (normal to the domain-wall plane). The unit magnetization vector $\boldsymbol{m}$ is determined in the angular coordinate system of Fig. 3, $(\theta; \phi)$, as $\mathbf{m} = (\sin\theta\cos\phi, \sin\phi, \cos\theta\cos\phi)$. The inhomogeneous magnetoelectric interaction ε_{ME} can be rewritten in the following form:

$$\varepsilon_{ME} = PM_s^2 \left[(\gamma_1 \cos^2\phi + \gamma_2 \sin^2\phi)\cos\theta \frac{d\phi}{dy} \right.$$
$$\left. + \gamma_2 \sin\theta \sin\phi \cos\phi \frac{d\theta}{dy} \right]. \quad (2)$$

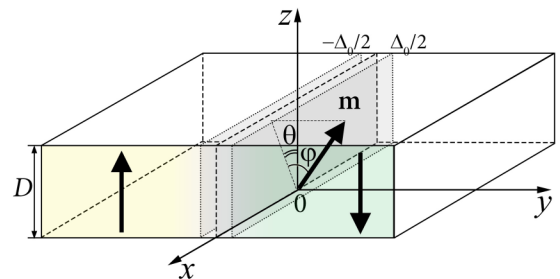The energy density of the magnetic inhomogeneities (namely, the total energy reduced to the sectional area film

FIG. 3. The geometry of the problem: Two domains with unit magnetization $\boldsymbol{m}$ are separated by a domain wall with a characteristic width parameter Δ_0. The $(\theta; \phi)$ angles show the magnetization rotation across the domain wall for Bloch and Néel components, respectively.

xOz) is written in the following form,

$$E = \int_{-\infty}^{+\infty} \left\{ A\left[\left(\frac{d\phi}{dy}\right)^2 + \cos^2\phi \left(\frac{d\theta}{dy}\right)^2 \right] \right.$$
$$+ K_u(\sin^2\theta\cos^2\phi + \sin^2\phi)$$
$$\left. + \varepsilon_{ME} + \varepsilon_H + 2\pi M_s^2 \sin^2\phi \right\} dy, \qquad (3)$$

where A is an exchange stiffness parameter, K_u is an uniaxial anisotropy constant, ε_{ME} is an energy density of the inhomogeneous magnetoelectric interaction Eq. (2), and $\varepsilon_H = -M_s(\mathbf{m} \cdot \mathbf{H})$ is the Zeeman's energy density in an external field H.

We assume that the film is thick enough ($D \gg \Delta_0$, where $\Delta_0 = \sqrt{A/K}$ is the characteristic size of the domain wall determined by the competition between the exchange and magnetic anisotropy in the absence of an electric field) and neglect the contribution of the demagnetizing fields arising due to the effective magnetic surface charges. At the same time the demagnetizing fields' energy density due to the volume charges is described by the last term of Eq. (2) [20–22].

The structure and properties of magnetic inhomogeneities are determined from the Euler-Lagrange equations, which correspond to the minimum energy (1), and have the form

$$\frac{d}{d\xi}\left(\cos^2\phi \frac{d\theta}{d\xi}\right) - \sin\theta\cos\theta\cos^2\phi$$
$$+ (\mathcal{E}_1 + \mathcal{E}_2)\sin\theta\cos^2\phi \frac{d\phi}{d\xi}$$
$$- \frac{1}{M_s H_u}\frac{\partial\varepsilon_H}{\partial\theta} = 0,$$

$$\frac{d^2\phi}{d\xi^2} - \sin\phi\cos\phi\left[\cos^2\theta - \left(\frac{d\theta}{d\xi}\right)^2\right]$$
$$- (\mathcal{E}_1 + \mathcal{E}_2)\sin\theta\cos^2\phi \frac{d\theta}{d\xi}$$
$$+ \frac{1}{M_s H_u}\frac{\partial\varepsilon_H}{\partial\theta} - Q^{-1}\sin\phi\cos\phi = 0, \qquad (4)$$

where $\mathcal{E}_i = \frac{P}{E_i}$, $E_i = \frac{2K_u\Delta_0}{M_s^2\gamma_i}$, $i = 1, 2$; $\xi = \frac{y}{\Delta_0}$, $Q = \frac{K_u}{2\pi M_s^2}$. $\mathcal{E}_i$ and E_i are dimensionless and characteristic electric fields, ξ is a dimensionless coordinate, Q is the material's quality factor, and $H_u = 2K_u/M_s$ is the uniaxial anisotropy field. Further on, we use an additional dimensionless parameter, the reduced magnetic field $h = H/H_u$.

The solution of Eq. (4) with boundary conditions corresponding to two domains with opposite orientations of magnetization is a 180° domain wall with a noncircular trajectory of the magnetization vector $\mathbf{m}(y)$.

In the isotropic case, the magnetoelectric constants are equal, $\gamma_i = \gamma_1 = \gamma_2 = \gamma$, which means $\mathcal{E}_i = \mathcal{E}_1 = \mathcal{E}_2 = \mathcal{E}$. The electric polarization of the domain wall is determined from the thermodynamics as a derivative of the whole energy with respect to the electric field. The dimensionless domain-wall linear charge density that we use as a measure of magnetoelectricity of the domain wall can be found as an
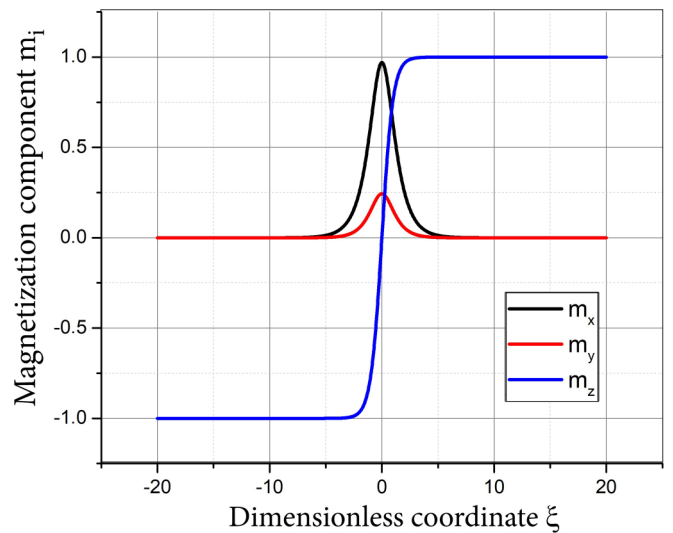
(a) $\mathcal{E} = 0.1$ $h_y = 0$
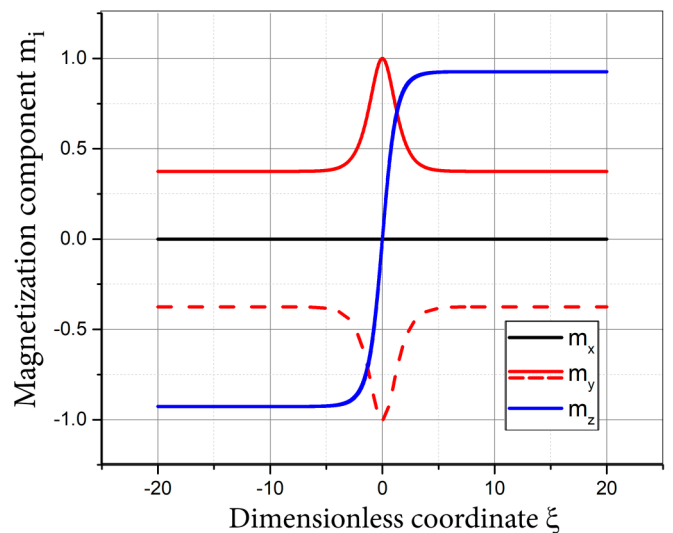
(b) $\mathcal{E} = 0.1$ $h_y = \pm 1$

FIG. 4. The calculated domain-wall profiles corresponding to the solution of Eq. (4). The components of the magnetization direction are shown in the absence of magnetic bias ($h_y = 0$) and in the presence of an in-plane magnetic field ($h_y = \pm 1$) that suppresses the Bloch component of the domain wall and induces a counterclockwise or clockwise Néel-type rotation of magnetization in the domain wall [the solid red line and the dashed red one in (b), respectively]. $\mathcal{E}$ is the dimensionless electric field.

integral over the width of the domain wall [22]:

$$\rho = \int_{-\Delta_0/2}^{+\Delta_0/2} \{\mathbf{m}(y)\operatorname{div}\mathbf{m}(y) + \mathbf{m}(y) \times \operatorname{rot}\mathbf{m}(y)\} dy. \quad (5)$$

IV. RESULTS AND DISCUSSION

The solution of Eq. (4) corresponding to the 180° domain-wall profile in the absence of a magnetic field and nonvanishing "built-in" electric field of the film $\mathcal{E}$ is shown in Fig. 4(a), $H = 0$. It has a nearly Bloch-type structure with
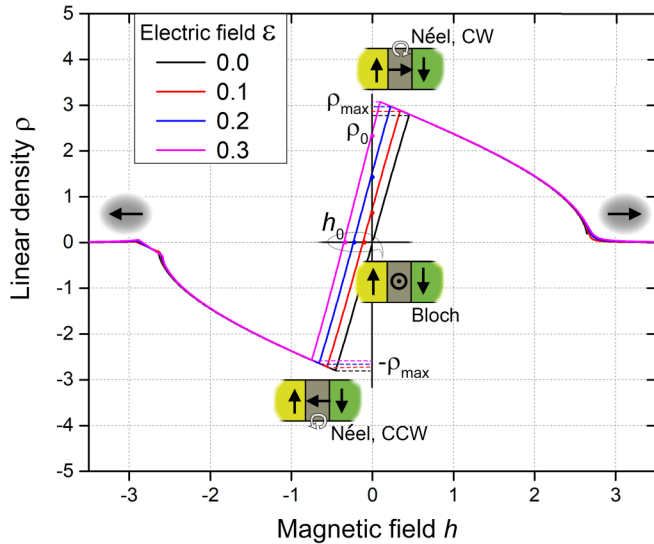
FIG. 5. The dimensionless linear charge ρ dependence on the reduced magnetic field h corresponding to various electric-field values $\mathcal{E}$. The schematics show the magnetization configuration at various fragments of the curves: The Bloch domain-wall state (at critical field h_0); the Néel domain walls with clockwise and counterclockwise (CW/CCW) magnetization rotation across the wall (at maxima/minima) of the curves ($\pm\rho_{max}$); and a single domain state with in-plane magnetization in high magnetic fields $|h| > 3$.

a slight Néel component due to the inversion symmetry breaking in the film.

The transformation of the domain wall in the external in-plane magnetic field $h = \pm 1$ perpendicular to the domain wall can be seen in Fig. 4(b). The Bloch component is suppressed completely, and the Néel-type magnetization rotation across the wall prevails. The direction of the rotation is either counterclockwise or clockwise depending on the sign of the in-plane projection of the magnetic field h_y [Fig. 4(b), solid and dashed lines, respectively]. A slight reduction of the magnetization component normal to the film is also seen. It can be attributed to the tilt of magnetization in the domains from the normal to the plane and the starting transition to the in-plane magnetized phase.

The domain-wall structure transformation affects the magnetoelectric properties of the domain wall. Figure 5 shows the results of numerical calculations for the linear charge density of the domain wall, as a function dependent on the applied external magnetic field $H||Oy$. The nonmonotonic dependence on the magnetic field reflects the transformation of the domain wall from a quasi-Bloch type to a Néel one and after that to the in-plane magnetized single domain state. At the extrema of the graphs, the domain wall becomes a completely Néel one and the decrease in polarization is associated with the transformation of the $180°$ domain wall to a domain wall with the reduced angle due to the tilt of magnetization in the domains along the field. In a certain field corresponding to $h > 2.5$ the magnetization falls into the plane and the domain wall disappears. The electric field leads to the shift of the magnetoelectric curves so that there is nonvanishing domain-wall polarization and a corresponding linear charge density ρ_0 in the absence of a magnetic field. The negative electric-
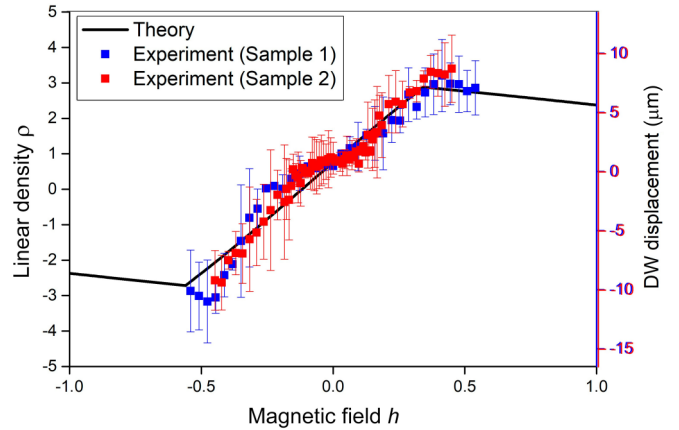

FIG. 6. The comparison with the experimental data. The black curve is the result of the numerical simulations of the linear charge density (left scale), and the blue and red points are experimental data for the electric-field-induced domain-wall displacement (right scale).

field values would result, respectively, in graphs with negative charge densities ρ_0 and opposite chirality of the domain wall. This electric-field-induced chirality switching was predicted in Ref. [23] and experimentally observed on $90°$ domain walls in Ref. [24]. However, in the case of our samples with a $180°$ domain wall we have not seen the negative linear charge densities and have not observed electric-field-induced chirality switching either, which is why the graphs for negative electric fields $\mathcal{E}$ are not shown.

Another special point of the graph is the critical magnetic field h_0 at which the switching of domain-wall chirality and electric polarization reversal occurs (Fig. 5).

The comparisons of the experimental and theoretical curves are based on several reference points characteristic of Fig. 5: (i) the critical field of the electric polarity reversal (h_0); (ii) the positive linear charge density ρ_0 of the domain wall in the spontaneous state (at zero magnetic field); and (iii) the maxima of the magnetoelectric effect corresponding to the pure Néel structure of the $180°$ domain wall ($\pm\rho_{max}$) and the starting transformation to the single domain in-plane magnetized state.

All these features can be observed on the experimental data in Fig. 6. Indeed, there is a nonzero electric-field-induced displacement of the domain wall even in the zero magnetic field that evidences for the spontaneous non-Bloch structure of the domain wall and its corresponding spontaneous electric polarization. There is also the disappearance of the magnetoelectric effect at some critical magnetic field, and its enhancement to the maximum values at the large magnetic field of both polarities.

To fit the experimental data with the results of the numerical simulation (Fig. 5) only one fitting parameter was used that characterizes the inversion symmetry breaking in the film, $\mathcal{E} = 0.1$, which corresponds to the effective electric field $E = 0.7$ MV/cm (the estimation is obtained in the assumption $\gamma \cdot M_s^2 = 10^{-6}\sqrt{\text{erg/cm}}$) [8].

Remarkably, two different samples follow the same theoretical trend [25] provided that the experimental magnetic field is normalized at $H_u = 2K_u/M_s$, where the effective

anisotropy constant K_u and magnetization M_s of the samples are used: $4\pi M_s = 54$ G, $K_u = 430$ erg/cm^3 for the first iron garnet film and $4\pi M_s = 77$ G, $K_u = 730$ erg/cm^3 for the second one.

V. CONCLUSION

Summarizing, the dramatic enhancement of the magnetoelectric properties of the domain wall in magnetic field was explained by a micromagnetic structure transformation of the domain wall from a quasi-Bloch type to a pure Néel one. The fitting of the experimental data by a theoretical curve enabled us to estimate the parameter

of the effective "built-in" electric field $E = 0.7$ MV/cm, which is related to the growth-induced asymmetry of the sample.

[1] M. Fiebig, T. Lottermoser, D. Meier, and M. Trassin, Nat. Rev. Mater. **1**, 16046 (2016).

[2] N. A. Spaldin, Proc. R. Soc. A **476**, 20190542 (2020).

[3] J. F. Scott, J. Mater. Chem. **22**, 4567 (2012).

[4] A. P. Pyatakov and A. K. Zvezdin, Phys. Usp. **55**, 557 (2012).

[5] J. Wu, Z. Fan, D. Xiao, J. Zhu, and J. Wang, Prog. Mater. Sci. **84**, 335 (2016).

[6] A. P. Pyatakov, A. S. Sergeev, E. P. Nikolaeva, T. B. Kosykh, A. V. Nikolaev, K. A. Zvezdin, and A. K. Zvezdin, Phys. Usp. **58**, 981 (2015).

[7] I. S. Veshchunov, S. V. Mironov, W. Magrini, V. S. Stolyarov, A. N. Rossolenko, V. A. Skidanov, J.-B. Trebbia, A. I. Buzdin, P. Tamarat, and B. Lounis, Phys. Rev. Lett. **115**, 027601 (2015).

[8] D. P. Kulikova, T. T. Gareev, E. P. Nikolaeva, T. B. Kosykh, A. V. Nikolaev, Z. A. Pyatakova, A. K. Zvezdin, and A. P. Pyatakov, Phys. Status Solidi RRL **12**, 1800066 (2018).

[9] A. Logginov, G. Meshkov, A. Nikolaev, E. Nikolaeva, A. Pyatakov, and A. Zvezdin, Appl. Phys. Lett. **93**, 182510 (2008).

[10] A. P. Pyatakov, T. T. Gareev, A. S. Kaminskiy, K. S. Antipin, E. P. Nikolaeva, D. P. Kulikova, A. S. Sergeev, and A. V. Nikolaev, in *Chirality, Magnetism and Magnetoelectricity: Separate Phenomena and Joint Effects in Metamaterial Structures*, edited by E. Kamenetskii (Springer, Cham, 2021), pp. 127–146.

[11] M. Mostovoy, Phys. Rev. Lett. **96**, 067601 (2006).

[12] P. I. Karpov and S. I. Mukhin, Phys. Rev. B **95**, 195136 (2017).

[13] A. Pyatakov, D. Sechin, A. Sergeev, A. Nikolaev, E. Nikolaeva, A. Logginov, and A. Zvezdin, Europhys. Lett. **93**, 17001 (2011).

[14] G. Arzamastseva, A. Balbashov, F. Lisovskii, E. Mansvetova, A. Temiryazev, and M. Temiryazeva, J. Exp. Theor. Phys. **120**, 687 (2015).

[15] B. Krichevtsov, V. Pavlov, and R. Pisarev, JETP Lett. **49**, 535 (1989).

[16] V. V. Pavlov, R. V. Pisarev, A. Kirilyuk, and T. Rasing, Phys. Rev. Lett. **78**, 2004 (1997).

[17] V. Bar'yakhtar, V. G. L'vov, and D. Yablonski, JETP Lett. **37**, 673 (1983).

[18] A. Sparavigna, A. Strigazzi, and A. Zvezdin, Phys. Rev. B **50**, 2953 (1994).

[19] I. Dzyaloshinskii, Europhys. Lett. **83**, 67001 (2008).

[20] A. Hubert and R. Schäfer, *Magnetic Domains: The Analysis of Magnetic Microstructures* (Springer, Berlin, 2008).

[21] E. B. Magadeev and R. M. Vakhitov, Theor. Math. Phys. **171**, 862 (2012).

[22] R. Vakhitov, Z. Gareeva, R. Solonetsky, and F. Mazhitova, Phys. Solid State **61**, 1043 (2019).

[23] H.-B. Chen, Y.-H. Liu, and Y.-Q. Li, J. Appl. Phys. **115**, 133913 (2014).

[24] K. S. Antipin, T. T. Gareev, N. V. Myasnikov, E. P. Nikolaeva, and A. P. Pyatakov, J. Appl. Phys. **129**, 024103 (2021).

[25] It should be noted, however, that the experimental points do not follow completely the theoretical linear trend due to the nonlinearity of the process of the domain-wall chirality switching, i.e., the transformation of the micromagnetic structure from one sense of magnetization rotation to another. This nonlinearity manifests itself at negative magnetic fields in the tendency for the experimental points to align along the horizontal axis and then suddenly dive to the large values of repulsion displacements. To partially compensate for this nonlinearity the offset $\delta\rho = 0.5$ of the theoretical dependence was introduced.